frontiers in Earth Science

ORIGINAL RESEARCH
published: 05 June 2020
doi: 10.3389/feart.2020.00173

Magnetostratigraphy and Paleoenvironments of the Kuntila Lake Sediments, Southern Israel: Implications for Late Cenozoic Climate Variability at the Northern Fringe of the Saharo-Arabian Desert Belt

Juan Cruz Larrasoaña[1], Nicolas Waldmann[2], Steffen Mischke[3], Yoav Avni[4] and Hanan Ginat[5]*

[1] Instituto Geológico y Minero de España, Unidad de Zaragoza, Zaragoza, Spain, [2] Department of Marine Geosciences, University of Haifa, Haifa, Israel, [3] Institute of Earth Sciences, University of Iceland, Reykjavík, Iceland, [4] Geological Survey of Israel, Jerusalem, Israel, [5] The Dead Sea and Arava Science Center, Tamar Regional Council, Mount Masada, Israel

OPEN ACCESS

Edited by:
Kenneth Philip Kodama, Lehigh University, United States

Reviewed by:
Josep M. Pares, National Research Center on Human Evolution, Spain
James G. Ogg, Chengdu University of Technology, China

***Correspondence:**
Juan Cruz Larrasoaña
jc.larra@igme.es

Specialty section:
This article was submitted to Geomagnetism and Paleomagnetism, a section of the journal Frontiers in Earth Science

Received: *31 March 2020*
Accepted: *05 May 2020*
Published: *05 June 2020*

Citation:
Larrasoaña JC, Waldmann N, Mischke S, Avni Y and Ginat H (2020) Magnetostratigraphy and Paleoenvironments of the Kuntila Lake Sediments, Southern Israel: Implications for Late Cenozoic Climate Variability at the Northern Fringe of the Saharo-Arabian Desert Belt. Front. Earth Sci. 8:173. doi: 10.3389/feart.2020.00173

The Negev Desert in southern Israel hosts a number of late Cenozoic lacustrine and palustrine sedimentary sequences that attest for past wetter conditions in what today constitutes one of the driest deserts on Earth. These sequences are of special importance because the Negev Desert forms part of the Levantine Corridor, which was probably the only continental bridge that enabled initial out-of-Africa expansion of our genus *Homo*. Yet, the paleoclimatic significance of these sequences still remains unknown, mainly due to their uncertain (late Pliocene to early Pleistocene) age. Here we present a combined sedimentologic, paleontologic and magnetostratigraphic study of one of these sedimentary sequences, the so-called Kuntila Lake sediments, which was carried out at the 30 m-thick Kuntila Gate section in the Nahal Paran basin, southern Israel. Sedimentological evidence and ostracod faunas indicate that these sediments accumulated in a long-lasting lacustrine basin that underwent periodic lake-level variations. Magnetostratigraphic measurements enable the recognition of a normal (N1) and a reverse (R1) polarity zone in the lower and upper halves, respectively, of the Kuntila Gate section. Correlation of N1 to the Olduvai Subchron (1.778–1.945 Ma) appears as the most likely option in view of previously published ^{10}Be ages derived for the uppermost part of the Kuntila Member in nearby sections. The large errors associated with these ages, however, suggest that correlation of N1 to Subchron C2An.1n (2.582–3.032 Ma) is also possible. Although our results do not resolve the age of the Arava Formation, they unequivocally relate the Kuntila Lake sediments with a long period of enhanced climatic variability because the tops of both subchrons are associated with 400 kyr eccentricity maxima. The inferred wetter conditions in the Negev

Desert concurred, regardless of the age correlation, with periods of lake expansion in East Africa and clusters of short-lived expansions of the savannah throughout much of the Sahara. This would have facilitated the biogeographic connection between Africa and Eurasia, greening the path for the initial out-of-Africa dispersal of *Homo*. Further research on the Kuntila Lake sediments will be necessary to better determine the timing, extent and significance of such biogeographic connection.

Keywords: magnetochronology, Arava Formation, Pleistocene, Pliocene, *Homo* dispersal, Near East

INTRODUCTION

Magnetostratigraphy is a powerful tool to date sedimentary sequences that is based on the recognition of polarity intervals in the target sequence and their correlation to the Geomagnetic Polarity Timescale (GPTS, Gradstein et al., 2012). This is, in turn, mostly constructed through radiometric ages of sea-floor magnetic anomalies (Ogg, 2012) or astronomically-tuned reversals derived from cyclically-accumulated sedimentary successions (Hilgen et al., 2012). Magnetic stratigraphy has proven to be especially well-suited for dating continental sedimentary successions, where the general scarcity of fossil remains or intercalations of volcanic material (e.g., tephra) usually makes obtaining well-resolved age models by biostratigraphic and radiometric methods difficult. Thus, magnetostratigraphic data have been paramount for providing the basic chronostratigraphic framework for continental sediments worldwide [e.g., East and North Africa (Lepre et al., 2011; Sahnouni et al., 2018), Chinese Loess Plateau (Zhu et al., 2018), and the Nihewan Basin (Deng et al., 2008)]. Independent magnetostratigraphic dating can be achieved if a single correlation of the local polarity sequence to the GPTS can be proposed, a situation that is more likely to occur as the length of the sedimentary succession increases the distinctiveness of the polarity pattern (provided that sedimentation rates are rather constant). For short sections with a limited number of reversals, magnetostratigraphy can still provide very valuable chronological data provided some independent age constraint is available to anchor the local polarity sequence (e.g., Lepre et al., 2011; Sahnouni et al., 2018).

This latter situation might be the case of the Arava Formation in the Negev Desert of southern Israel, which is typified by interbedded lacustrine and alluvial sediments accumulated within the so-called Kuntila Lake basin (Avni et al., 2001; Ginat et al., 2018; **Figure 1**). These sediments are cropping out over an area of circa 300 km^2 exposed in the transition between the eastern Sinai Peninsula and the southern Negev, and their age is still unknown despite its relevance for understanding the environmental setting in the only land bridge that made the initial African dispersal of our genus *Homo* possible without involving seafaring (Anton et al., 2014). Attempts to date these sediments by cosmogenic burial methods rendered unreliable results (Guralnik, 2009), and at present only numerical ages derived from ^{10}Be data are available for the desert pavement developed on the conglomerate beds that resumed sedimentation in Kuntila Lake (Matmon et al., 2009; Guralnik et al., 2010; Amit et al., 2011). These data give a minimum age of 1.83 $\pm$ 0.2 Ma for the Kuntila Lake sediments, yet the large errors associated with cosmogenic exposure ages, coupled with uncertainties and assumptions behind their calculation (Matmon et al., 2009), result in a still somewhat uncertain age for these sediments.

Here we present a magnetostratigraphic study of the Kuntila Lake sediments at the Kuntila Gate (KG) section. Despite the relatively small thickness of the section (30 m), our results provide some important constraints for the age of these sediments. These constraints, combined with new sedimentological and paleontological evidence, enable an improved discussion on the paleoenvironmental significance of the Kuntila Lake sediments.

GEOLOGICAL SETTING

The Negev Desert in southern Israel is located between the Sinai Peninsula and the Dead Sea Basin, at the northernmost fringe of the Saharo-Arabian desert, and belongs to the only continental bridge that joins Africa to Eurasia (**Figure 1**). It is characterized by an arid to hyper-arid climate with a mean annual rainfall ranging from 200 mm in its northern part to less than 25 mm in its southern sector (Enzel et al., 2008). This situation results from a decreased southward penetration of the westerly winter rains brought to the region by eastern Mediterranean low-pressure systems (Enzel et al., 2008). Changes in the intensification of the Cyprus Low associated to North Atlantic climate shifts are considered as the main mechanism driving climate variability in the Negev during the Quaternary (Ziv et al., 2006; Enzel et al., 2008), although some studies contest this hypothesis and suggest that northward intrusion of tropical rains during boreal summers might also have played a role in contributing to wetter conditions during past interglacial periods (Vaks et al., 2007; Waldmann et al., 2010; Orland et al., 2019).

The geology of the region is dictated by the Miocene establishment of the Dead Sea Transform system, a fault system with a half-graben topography and a left-lateral motion that represents the boundary between the African and Eurasian plates (Garfunkel, 1981; Avni et al., 2012). This system led to formation of a central depression, represented by the Arava Valley, that was bounded by an uplifted eastern rift margin (the Trans-Jordan mountain belt) and by an arched and subsided western counterpart (the Negev Desert). Development of this transform system and the uplift of its shoulders led to the disruption of an initial regular topography developed during the Oligocene-Early Miocene (Avni et al., 2012), so that a new fluvial system was established draining the eastern part of the northern Sinai

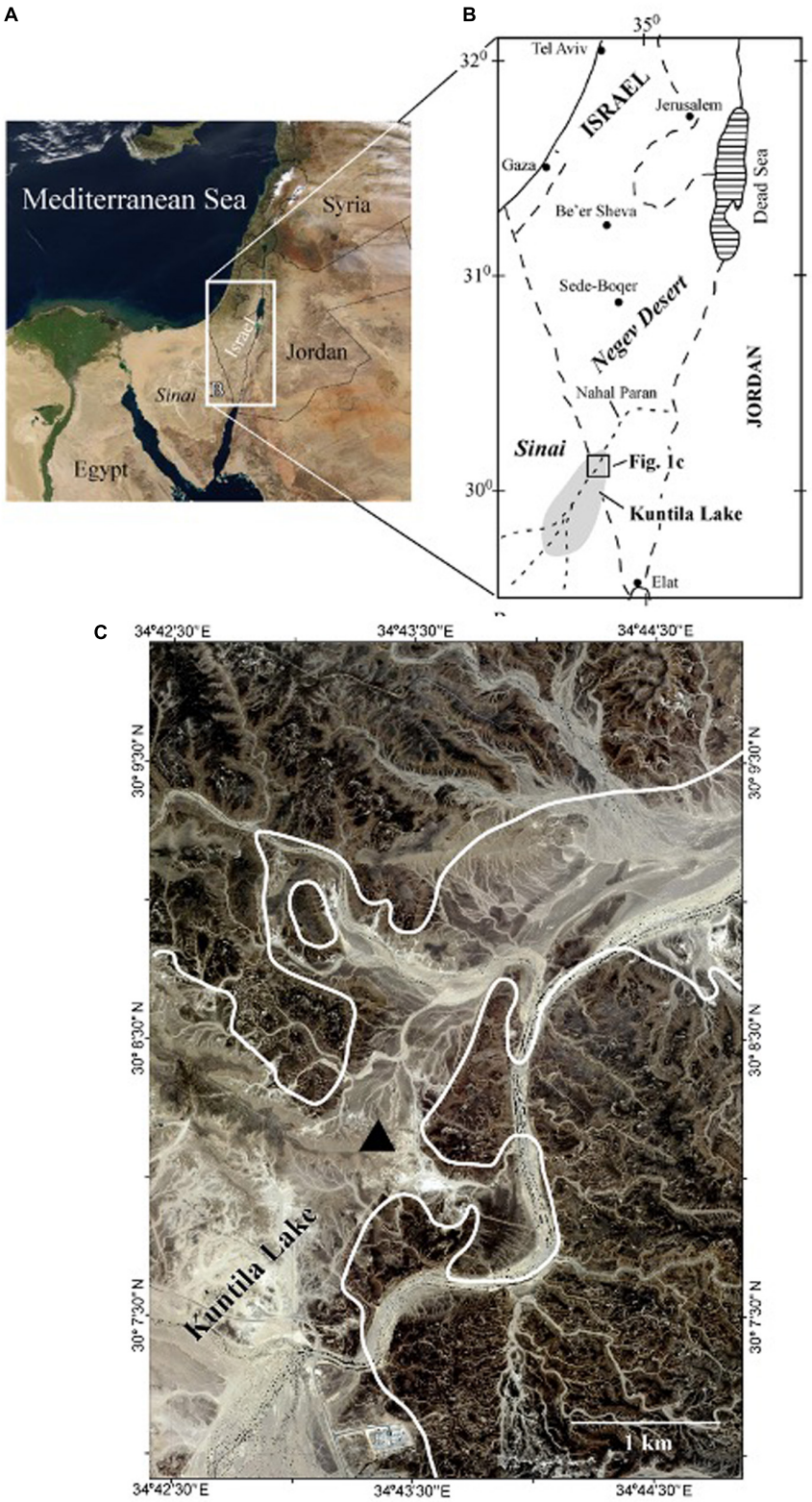

FIGURE 1 | (A) Satellite image showing the location of the Sinai Peninsula at the biogeographic bridge between Africa and Eurasia. The white rectangle is enlarged in **(B)** and depicts a sketch map of southern Israel with the inferred extension of the Kuntila Lake. **(C)** Satellite image of the Nahal Paran basin in the southern Negev Desert, with location of the Kuntila Gate section (black triangle). The thick white line delineates the outcrops of the Kuntila lacustrine sediments within the Arava Formation in the area.

Peninsula and much of the Negev northward into the young Dead Sea Basin (Avni et al., 2000). Evidence of this drainage system is provided by sediments of the Arava Formation, which accumulated after a period of extensive erosion associated with the initial rearrangement of the drainage network (Avni et al., 2000, 2001; **Figure 2**). Tectonic activity during the early Pleistocene faulted and tilted the Negev margin toward the east, hence terminating sedimentation of the Arava Formation and leading to the erosion of its uppermost strata at some locations (Avni et al., 2001). Deposition of the overlying Zehiha Formation took place broadly simultaneously with this period. Later incision of the newly formed drainage network led to deposition of Middle to Late Pleistocene alluvial terraces that also truncate previous deposits (Avni et al., 2001; Guralnik et al., 2010).

The Arava Formation has been formally described by Avni et al. (2001) to account for the sedimentary sequences deposited in the Negev and the Arava Valley after the Late Miocene birth of the Dead Sea Basin, and is composed of two members. The first one (Saggi Member) is made up of 5–20 m of poorly cemented conglomerate beds that include boulders of up to 2 m in diameter and were deposited along fluvial channels with a flash-flood hydrological regime. The second member (named Kuntila) was deposited after a short period of tectonic deformation and incision at a lower morphostratigraphic position (**Figure 2**). The Kuntila Member ranges in thickness between 30 and 80 m, and is made up of conglomerates, sandstones, mudstones, marls, and limestones. Mudstones, marls and limestones constitute a sequence of up to 35 m that attest to a lacustrine/palustrine setting along the course of the reconstructed paleo Paran-Neqarot drainage basin (Avni et al., 2000, 2001). Mapping of these sediments revealed that the largest lake, termed the Kuntila Lake, which had an elongated North-South direction and extended from the present-day Paran River well into the Egyptian side of the Sinai Peninsula, covered an area of more than 300 km^2 (Avni et al., 2001; Ginat et al., 2018; **Figure 1B**). Lacustrine sediments grade toward the periphery of the former lake basin into conglomerates, sandstones and mudstones of alluvial origin (Avni et al., 2001). Two main climatic scenarios have been proposed to explain the past occurrence of this and other water bodies scattered in the present-day hyper-arid Negev Desert (Ginat et al., 2018). The first scenario involves the alternating hyper- to semi-arid conditions, whereas the second implies fluctuations between hyper-arid and sub-humid conditions (Ginat et al., 2018). Although regional considerations suggest that the first scenario is more likely, the debate is still ongoing and new data are necessary to furnish our knowledge on the underlying mechanisms for this climatic variability (Ginat et al., 2018).

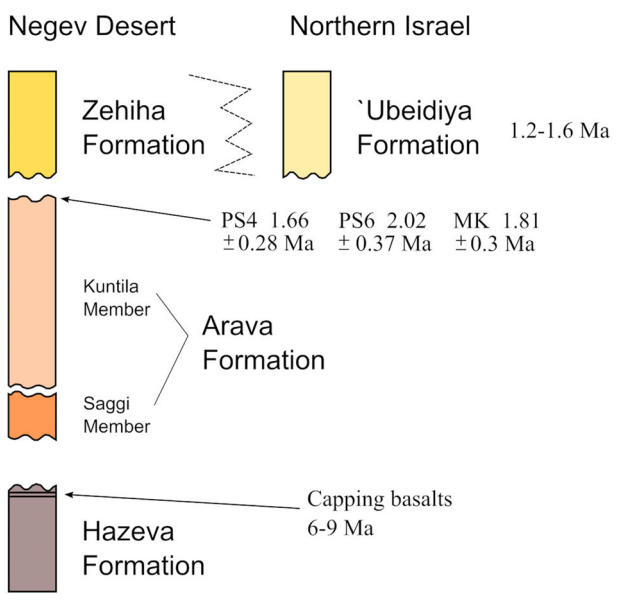

FIGURE 2 | Sketch showing the arrangement and lateral equivalences of the different formations discussed in the text. PS4, PS6 and MK indicate exposure ages (Matmon et al., 2009; Amit et al., 2011; Guralnik et al., 2010).

The age of the Arava Formation has been classically assigned from its geologic and geomorphological context. Thus, this formation post-dates the Hazeva Formation and its capping basalt flows, which have been dated to 9–6 Ma (Avni et al., 2001; **Figure 2**). It is, in turn, overlain by the Zehiha Formation, for which a similar age to the 'Ubeidiya Formation (which ranges between 1.2 and 1.6 Ma; Belmaker, 2010; Parés et al., 2013) has been proposed on the basis of its faunal assemblage (Ginat et al., 2003). All in all, the geological and geomorphological context points to a late Pliocene-early Pleistocene age for the Arava Formation (Avni et al., 2000). It has not been until the last decade that absolute chronological methods have been applied to determine the age of the upper member of the formation, the Kuntila Member. Efforts in providing numerical ages based on cosmogenic burial analyses have yielded unreasonable ages due to problems in extracting and measuring ^{26}Al in the studied sediments (Guralnik, 2009). Successful results have been provided, in contrast, by ^{10}Be exposure ages of a desert pavement developed on the reg soils that were formed, in turn, over the gravels that represent the last stages of sedimentation of the Kuntila Lake sediments (Matmon et al., 2009). Initial ages for sites PS4 and PS6 (Matmon et al., 2009) have been recalculated by Amit et al. (2011) to 1.66 ± 0.28 and 2.02 ± 0.37 Ma, respectively. Guralnik et al. (2010) added a third site (KM) from a similar position at the top of a Kuntila Member conglomerate sequence, located 28 km north-east of our KG section, with an age of 1.81 ± 0.3 Ma. These ages, therefore, provide a minimum age estimate that points to accumulation of the Kuntila Lake sediments sometime in the very early Pleistocene, yet this chronology should be considered with caution for three main reasons. First, these ages differ by up to 0.36 Myr despite the fact they were obtained almost at the same stratigraphic position. Second, the uncertainty associated to each individual age are rather wide (up to 0.74 Myr). And third, uncertainties and assumptions behind exposure-age calculations are noticeable, so that the initial age for site PS4 given by Matmon et al. (2009), which ranged between 1.75 and 2.35 ± 0.2 Ma depending on model input parameters, was later recalculated to 1.61 ± 0.26 and 1.66 ± 0.28 Ma by Guralnik et al. (2010) and Amit et al. (2011), respectively. It is clear that further dating techniques need to be

applied to better constrain the age of the Kuntila Lake sediments, with magnetochronology appearing as an obvious one.

MATERIALS AND METHODS

We have logged and described the lithology of the Kuntila Member sediments that crop out horizontally at the KG section in the Paran-Neqarot Basin, including description of color, grain size, bed thickness, and sedimentary structures and textures (Avni, 1998; Avni et al., 2001; **Figure 3**). We have selected this section because it includes some of the thickest and better exposed fine-grained lacustrine sediments within the sequence (Avni et al., 2001), and hence render optimal conditions for retrieving a local magnetozone succession. This information has been used to complement the observations made by Avni (1998) and Avni et al. (2001), and provide a revised view on the paleoenvironments of the Kuntila Lake sediments as inferred from basic sedimentological evidence.

Standard paleomagnetic samples were collected in the field using a battery-powered electric-drill equipped with a diamond drill-bit that was lubricated and cooled with water during sampling. A total of 19 samples were collected at 17 sites distributed throughout the section, giving an average stratigraphic resolution of ca. 1.7 m. We focused our sampling on mudstones and marls although some limestones and sandstones were also sampled. The samples were oriented in the field using a magnetic compass mounted on a paleomagnetic orienting fixture. After cutting the samples into standard paleomagnetic specimens and labeling, we conducted paleomagnetic analyses at the Paleomagnetic Laboratory of the Institute of Earth Sciences Jaume Almera (CCiTUB-CSIC) in Barcelona, Spain. A 2G superconducting rock magnetometer with a noise level of $< 7 \times 10^{-6}$ A/m was used to measure the Natural Remanent Magnetization (NRM) of the studied samples upon thermal demagnetization, which was conducted with a MMTD–80 furnace at intervals of 100, 50, 30, and 20°C, to a maximum temperature of 620°C. Stable Characteristic Remanent Magnetization (ChRM) directions were calculated by means of Principal Component Analysis (Kirschvink, 1980) after they were identified through visual inspection using the VPD software (Ramón et al., 2017).

In order to provide new paleoenvironmental information, we have also studied calcareous microfossils, mainly ostracod valves, at 23 stratigraphic levels distributed throughout the KG section. From each level, sediment sub-samples of 75–320 g (average 130 g) were treated with 3% H_2O_2 for 48 h and washed through 100, 250, and 1000 μm sieves. All ostracod remains including partly fragmented valves larger than half of a specimen were picked from the sieve residues. Valves and carapaces were recorded separately. Their preservation state was assessed as recrystallized or relatively well-preserved specimens. The portions of carapaces to all recorded valves (articulated and separated), and adult to all recorded valves were determined as proxies of post-mortem transport and preservation. Identification was conducted according to Meisch (2000), Fuhrmann (2012) and Meisch et al. (2019). Identification of *Ilyocypris* cf. *bradyi* Sars, 1890 followed van Harten (1979) by examining marginal ripplets on the inner lamella of left valves with a Zeiss Supra 40 VP Scanning Electron Microscope (SEM) at Freie Universität Berlin, Germany. In addition to ostracod remains, gastropod and bivalve shells, and charophyte remains were counted. Foraminifera tests were regarded as allochthonous, originating from locally exposed marine limestones of Maastrichtian to Paleocene age, and were qualitatively recorded.

RESULTS

Stratigraphy and Sedimentology

The Kuntila Member at the KG section (**Figure 3**) begins with a 2 m-thick package of massive, gray mudstones that is overlain by 5 m of also massive, gray-brownish silty mudstones. The following 2 m are composed of reddish sandy mudstones that include two tabular sandstone beds displaying low-angle cross bedding lamination (**Figure 4A**). Above them, about 4 m of massive, silty sands with thin reddish mudstone intercalations appear, with sands in the uppermost meter being indurated by carbonate cement. The next 5 m of the section are made up by three packages constituted by marls and a limestone bed each. Marls are gray in color, have an overall massive appearance, and include frequent organic debris at some darker gray horizons. Limestone beds range between 30 and 100 cm in thickness, display a tabular geometry with some occasional wavy morphology, and often have bioturbated tops (**Figure 4B**). These limestones are typically massive and contain remains of gastropods and charophytes. The uppermost limestone bed is overlain by 7 m of ochre sandy mudstones with occasional carbonate nodules in their upper part (**Figure 4C**). These sandy mudstones include two tabular, fining-upward conglomerate beds of around 50 and 100 cm in thickness. Clasts are well rounded, have a maximum size of 25 cm, and are mainly composed of carbonates, although chert and magmatic compositions are also found. The next 4.5 m of the section are characterized by sandy mudstones and sandstones with a silty matrix that show distinctive features such as color mottling, carbonated rhizoliths, and some gypsum gastropod steinkerns. The Kuntila Member is here erosively truncated by the Zehiha Formation, which is composed by a 1.7 m-thick conglomerate at the studied section (**Figure 4D**).

Fossil Remains

In total, 411 ostracod carapaces and 329 valves were identified in the sediments of the KG section. Ostracod remains are dominated by carapaces and valves of *Cyprideis torosa* (Jones, 1850; 56%). Carapaces and valves of *Neglecandona angulata* (Müller, 1900) occurred as the second most abundant ostracod remains (24%), followed by those of *Ilyocypris* cf. *bradyi* (8%) and *Neglecandona neglecta* (Sars, 1887; 7%; **Supplementary Plate S1**). Remains of seven additional ostracod taxa were recorded with very low abundances (**Supplementary Plate S2**). Relatively abundant ostracod remains in addition to those of *C. torosa* were only recorded in two samples from the basal and middle part of the KG section, respectively (**Figure 5**). Shells of four gastropod taxa were

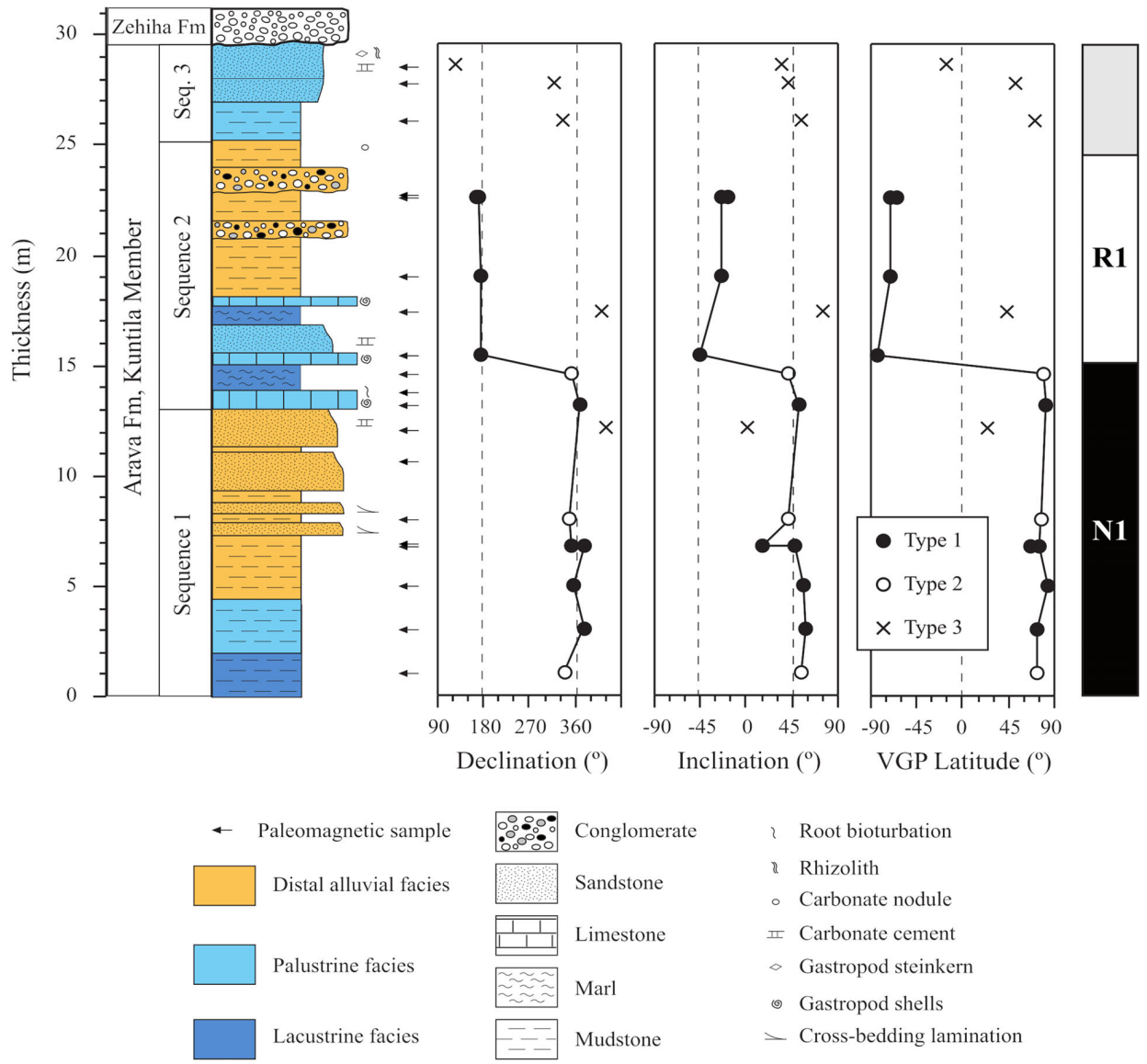

FIGURE 3 | Stratigraphic log of the Kuntila section, magnetostratigraphic results and the sequence of polarity zones identified in the section. The gray bar marks the position of the part of the sequence with uncertain polarity.

recorded in three samples, a shell of a bivalve in one sample, and gyrogonites of two *Chara* species in five samples (**Figure 5** and **Supplementary Plate S2**). All apart from two samples contain foraminifera tests, which attest to the contribution of eroded Maastrichtian-Paleocene chalk and marl sediments.

Magnetic Stratigraphy

The paleomagnetic quality of the samples is, overall, relatively good (see **Supplementary Tables S1, S2**). A low temperature component is typically identified between 100 and 225°C after removal of a viscous overprint. This low-temperature component shows northerly directions and positive, steep inclinations that are consistent with the present-day field overprint (**Figure 6**). Above 225–300°C, an additional stable component that unblocks below 590°C (occasionally up to 620°C) has been identified at most of the samples. This component is interpreted as the ChRM and can be divided into three types on the basis of quality. Type 1 ChRM directions are those that define strikingly linear trends directed toward the origin of the demagnetization plot, enable optimum polarity determination, and are associated with low mean angular deviation (MAD) angles (typically $< 8°$; **Figures 6A,D,E**). Type 2 ChRMs are characterized by either less linear trends or incomplete demagnetization due to the growth of new magnetic minerals in the oven. Despite this, they enable accurate calculation of ChRM directions with low to moderate MAD angles (typically between 10 and 20°) and reliable polarity determinations (**Figure 6C**). Type 3 ChRMs are characterized by lower intensities and scattered directions that provide ambiguous

FIGURE 4 | Field pictures of the studied sediments from the Kuntila Member of the Arava Formation. **(A)** Overall view of the lower part of the KG section, which encompasses sediments from S1 capped by the first limestone bed of S2. **(B)** Detail of the lacustrine limestone. **(C)** View of the ochre sandstones from the middle part of S2. **(D)** Conglomerate of the Zehiha Formation, erosively truncating the uppermost part of S3.

polarity determinations (**Figure 6B**); they were, therefore, not considered for establishing the local magnetozone succession. A total of nine, three and five ChRM directions display quality types 1, 2, and 3, respectively.

About half of the ChRM type 1 and 2 directions show northerly declinations with positive inclinations that appear well clustered in a stereographic projection around the expected direction for the studied site (**Figures 3**, **6F**). The rest of the ChRM type 1 and 2 directions show southerly declinations with negative inclinations of ca. −28° (**Figures 3**, **6F**). In the absence of a statistically significant reversal test, these circumstances suggest that the ChRM is a dual polarity, primary magnetization in which the reverse directions are overlapped to a small degree with the present-day field component. This is further supported by the depth variations of the latitude of the virtual paleomagnetic poles calculated from the ChRM directions, which are unrelated to lithological variations and enable a straightforward delineation of a normal polarity interval (N1) spanning the lower part of the section and a reverse polarity interval (R1) spanning most of its upper part (**Figure 3**). Above meter 25, the presence of only type 3 directions renders determination of the polarity uncertain (marked with a gray bar in **Figure 3**).

DISCUSSION

Sedimentological and Paleoenvironmental Inferences

The Kuntila Member sediments at the KG section are arranged in three sequences (**Figure 3**). The lowermost sequence (S1, 0–13 m) begins with gray mudstones interpreted to represent sedimentation in a lacustrine area, that grade upward into ochre and reddish silty mudstones typical for distal alluvial facies, and finally to reddish silty mudstones with tabular sandstone intercalations that attest to deposition by unconfined flows over a muddy flood plain. The second sequence (S2, 13–25 m) begins with the return to lacustrine sedimentation, which involved development of a carbonate cement within the uppermost distal alluvial sandstones of the underlying sequence. The three marl-limestone packages are interpreted as three periods of lacustrine sedimentation (represented by the marls) that evolved gradually to shallower palustrine conditions (represented by limestones with frequent bioturbated tops). Sedimentation then shifted to a distal alluvial plain (as indicated by ochre sandy mudstones) over which progradation of more proximal alluvial facies (as indicated by the conglomerates) occurred. The third sequence (S3, 25.0–29.5 m) begins with the return to palustrine sedimentation under the influence of detrital supply, as evidenced by gray and ochre sandy mudstones and sands with carbonate nodules. Shallower palustrine conditions prevailed later, as inferred from development of carbonate rhizoliths within silty sands. The occurrence of mottling and gypsic gastropod steinkerns within these sediments attest to the cessation of palustrine conditions and its pedogenic alteration.

Before detailed paleoenvironmental information can be derived from the recorded ostracod remains, two considerations are taken into account. First, the relatively low number of adult valves in comparison to those of juvenile specimens (**Figure 5**) indicate that the valves were likely formed autochthonous and not brought to the site as detrital particles. Second, the high proportion of carapaces in comparison to disarticulated valves (**Figure 5**) might indicate rapid burial and preservation of articulated valves or, alternatively, might result from poor preservation conditions for the more fragile isolated valves in comparison to carapaces. The frequent appearance of only *Cyprideis torosa*, whose valves are thicker than those of most non-marine species, in several samples is supporting evidence for the second alternative and suggests that the recorded ostracod specimens represent only a part of the original ostracod assemblage. Highest proportions of carapaces in comparison to all valves, and of recrystallized valves in comparison to all valves, occur in the lower half of the section suggesting that poor preservation is more significant in the lower part (**Figure 5**).

The dominance of *Cyprideis torosa* forma *torosa* between meters 1 and 6 suggests the past presence of brackish water conditions and a permanent water body that agree with the lacustrine sedimentation inferred for the lower part of S1. The combined occurrence of *Cyprideis torosa* forma *torosa* and *Cypridopsis vidua* (Müller, 1776) between meters 13 and 15 points to slightly brackish conditions associated with deposition of the lacustrine gray marls and limestones found in the lower half of S2. The occurrence of charophyte gyrogonites together with relatively abundant ostracod remains in addition to those of *C. torosa* in the same stratigraphic positions confirm that the lower parts of S1 and S2 represent deposition in permanent fresh to slightly brackish and predominantly clear waters. However, at least slightly brackish or even more saline conditions existed in more or less stagnant waters when the fine-grained and

carbonate-rich deposits of the KG section were accumulated. This inference is indicated by the dominance of *C. torosa*, and in addition for S1 by the presence of valves of *N. angulata*, *N. neglecta,* and *Heterocypris salina* (Brady, 1868), and a shell of *?Melanopsis* (**Figure 5**). The occurrence of *Paralimnocythere* sp., *Cypris*, *Herpetocypris*, *Vestalenula cylindrica* (Straub, 1952), and *Gyraulus* sp. in a sample of S2 points to the existence of small, spring-fed water bodies, possibly representing a wetland rather than a lake environment. With respect to S3, only few valves of *C. torosa*, *H. salina* and *Ilyocypris* cf. *bradyi*, and gyrogonites of *Chara* sp. 2 were recorded in its lower part (**Figure 5**). The brackish water conditions inferred from these remains and the occurrence of pedogenic features (rhizoliths, carbonate concretions) support the reconstruction of mainly palustrine conditions during the formation of S3, and its cessation likely in association with enhanced evaporation as indicated by gypsum casts. The rest of the studied samples, collected from distal alluvial sediments, are barren in ostracod valves or other organism remains with the exception of that around meter 11, where a few recovered *C. torosa* remains resulted probably from brackish stagnant or slowly flowing conditions on an alluvial plain (**Figure 5**). A shallow oxbow-lake or in-stream wetland scenario is reconstructed here.

In summary, our results indicate that the Kuntila Member at the KG section is composed by two sequences (S1 and S2) that witnessed a gradual shallowing from lacustrine to palustrine and distal alluvial conditions, plus a third sequence (S3) devoid of the initial lacustrine part (**Figure 3**). Previous studies have reported the presence, in addition to the ostracod assemblage similar to those presented here, of fish remains of *Tilapia* and *Haplochromis* and gastropod remains of *Bulimis* and *Melanoides operculata* (Avni, 1998; Ginat et al., 2018). Although we are unaware of the exact stratigraphic position of fish remains within the succession, they further demonstrate the past presence of permanent, stagnant waters, and thus, most likely fully lacustrine conditions at least for the lower parts of S1 and S2. Such sediments accumulated under fully lacustrine conditions account for about a third of the stratigraphic thickness exposed at the KG section. Palustrine, likely brackish water conditions prevailed through another third of the section, and distal alluvial conditions account for the remaining third of the succession. The alternation of alluvial sedimentation with lacustrine and palustrine conditions at the KG section location does not necessarily imply disruption of a lacustrine setting in the region. The KG section is located near the former depocenter of the Kuntila Lake but close to its northern outlet toward the paleo-Paran-Neqarot River, where the lake was narrowest (Avni et al., 2001; **Figure 1**). Thus, retraction of the Kuntila Lake led to progradation of distal alluvial sediments over the former lake at the location of the KG section, whereas lacustrine sedimentation likely prevailed in the central sector of its wider, southernmost part. The tabular geometry of the sandstone and conglomerate beds observed in the KG section attest to deposition by unconfined flows in a low-gradient alluvial plain, which suggests continued aggradation throughout the basin in response to a stable base level likely represented by a terminal lake. Any subsequent expansion of the lake would have resulted in the return to lacustrine sedimentation throughout most of the basin and the concomitant retreat of alluvial facies. The succession of three expanding/retracting lacustrine/palustrine sequences suggests, under the relatively quiet tectonic scenario inferred for deposition of the Arava Formation (Avni et al.,

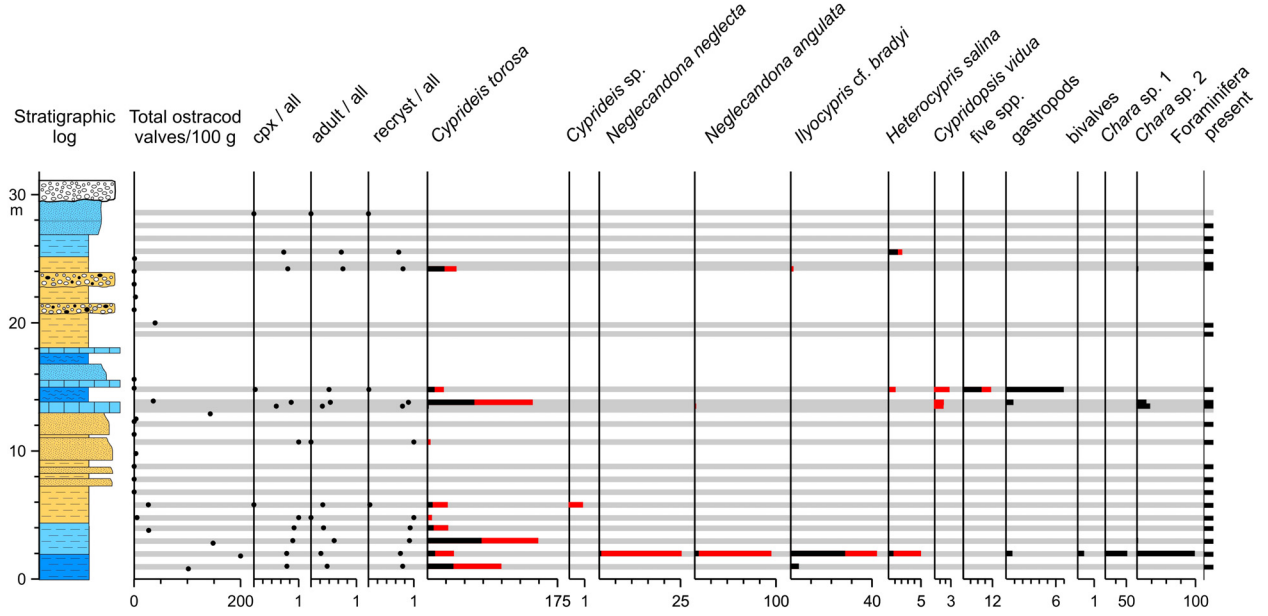

FIGURE 5 | Depth variations of relevant fossil remains from the Kuntila Lake sediments. The pooled five spp. are valves and larger fragments of the ostracods *Potamocypris* sp., *Vestalenula cylindrica*, *Paralimnocythere* sp., *Cypris* sp., and *Herpetocypris* sp. The gastropods are shells of *Gyraulus* sp., Lymnaeidae, *?Melanopsis* and *?Valvata*. Gray horizontal bars indicate the positions of samples.

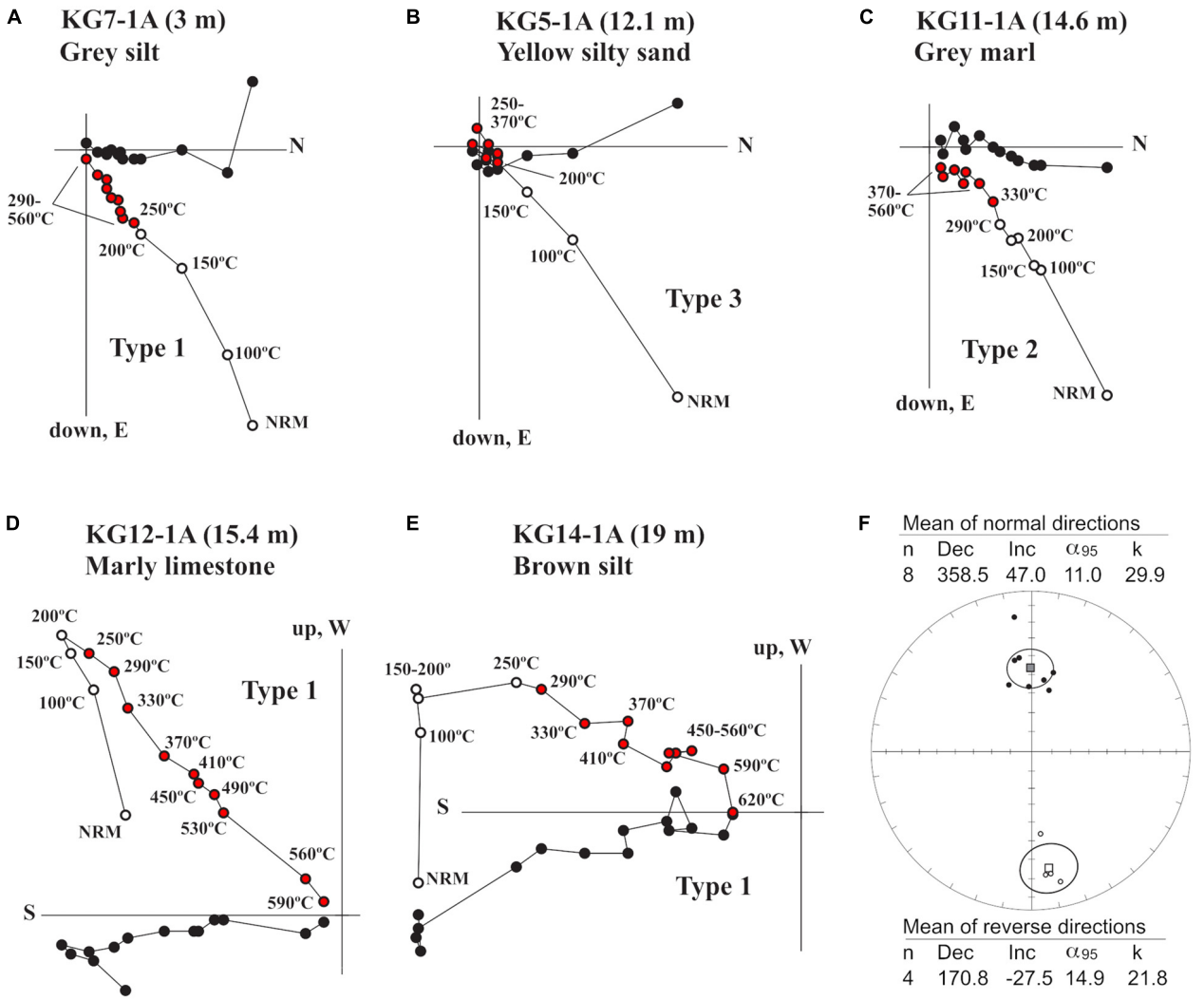

FIGURE 6 | Orthogonal demagnetization plots of samples representative for Type 1 **(A,D,E)**, Type 2 **(C)** and Type 3 **(B)** behaviors. Black and white dots represent projections in the horizontal and vertical planes, respectively. Red dots in the vertical projections indicate the temperature steps included in the calculation of the ChRM directions. **(F)** Equal-area stereonet projection of individual samples (circles), along with the mean directions and associated statistics of the normal and reverse polarity samples (squares). Bold (open) symbols represents projection in the lower (upper) hemisphere. Only types 1 and 2 samples have been considered for the calculations.

2001), that climatic variations were responsible for altering the hydrological budget of the drainage system to the point of enabling the formation of a long-lasting open-water surface in the present hyper-arid southern Negev Desert.

Age of the Kuntila Lake Sediments and Paleoclimatic Implications

Correlation of the KG section magnetostratigraphy to the astronomically-tuned Neogene time scale (ATNTS2012, Hilgen et al., 2012) is not straightforward. Of the three ^{10}Be exposure ages obtained atop of the Kuntila Member, which provide minimum age estimates for the sequence, one of them (MK, 1.81 ± 0.3 Ma; Guralnik et al., 2010) gives an age within the Olduvai Subchron (1.778–1.945 Ma, Hilgen et al., 2012), whereas the others give an age either younger (PS4, 1.66 ± 0.28 Ma; Amit et al., 2011) or older (PS6, 2.02 ± 0.37 Ma; Amit et al., 2011) than this subchron (**Figure 7**). Moreover, the errors of all three exposure ages encompass the entire Olduvai Subchron. Therefore, although the most straightforward solution is to correlate our magnetozone N1 to Olduvai (Option 1, **Figure 7**), other possibilities cannot be excluded. An alternative assessment is the correlation of magnetozone N1 with the uppermost part of the Gauss Chron, named C2An.1n (2.582–3.032 Ma; Hilgen et al., 2012; Option 2, **Figure 7**). The fact that an undetermined part of the uppermost Kuntila Member has been eroded at the KG section before deposition of the Zehiha Formation obliges us to consider this correlation, since an age still older than that indicated by the exposure ages should be attributed to the top of the Kuntila Member in this section. A third alternative,

correlating N1 to the Reunion Subchron within C2r (2.129–2.149 Ma; Hilgen et al., 2012) is discarded due to the high sediment accumulation rates implied (e.g., >75 cm/kyr). In order to provide a definitive age for the Kuntila Member, new sections exposing a thicker sequence need to be sampled for magnetostratigraphic analyses. Drilling a core at the base of the KG section might also resolve the chronology of the Kuntila Member provided a sufficiently long section can be recovered and magnetostratigraphically dated. A final option would be to apply other dating methods (e.g., electron spin resonance) to quartz grains of detrital sediments of the Kuntila Member.

The tops of both subchrons Olduvai and C2An.1n are associated with two 400 kyr eccentricity maxima (Laskar et al., 2004; **Figure 7**). This is significant because it relates sedimentation of the Kuntila Lake sediments with a period of enhanced climatic variability regardless of the correlation of our N1 magnetozone to either of these two subchrons. Thus, eccentricity variations influence climate by modulating precession, so that maxima in eccentricity drive maxima in precession that result, in turn, in enhanced northern-hemisphere insolation values (Laskar et al., 2004). Such periods of highest northern-hemisphere insolation values have been demonstrated to intensify eastern Mediterranean low-pressure systems and their associated winter rains (Toucanne et al., 2015), and might be responsible for the overall shift to wetter conditions that led to development of the Kuntila Lake. Simultaneous intensification of southerly low- and mid-latitude rains during northern-hemisphere insolation maxima (Waldmann et al., 2010) likely contributed to enhance the hydrological balance of the southern Negev. Considering typical accumulation rates of lacustrine-distal alluvial sequences formed in arid and semi-arid zones (typically 7–15 cm/kyr; Ginat et al., 2003; Larrasoaña et al., 2006; Pérez-Rivarés et al., 2018), a total span of about 200–400 kyr might be estimated for the Kuntila Member, which would be entirely consistent with its accumulation around the high eccentricity half of a 400 kyr maximum, regardless of the proposed correlation. These inferences, along with sedimentological and paleontological evidence, reinforce the notion of a long-lasting open-water surface in the context of a climatic shift to, at least, semi-arid conditions in the present-day hyper-arid Negev Desert and surrounding areas (Ginat et al., 2018). In addition to permanent fresh-water bodies, it is very likely that the enhanced hydrological balance would have also led to the retraction of arid dryland at the expense of more vegetated ecotones, and to the at least partial reactivation of the fluvial network. These circumstances resulted, coupled with a tectonically-driven heterogeneous topography, in a dynamic landscape favorable for human occupation and migration (Bailey et al., 2011).

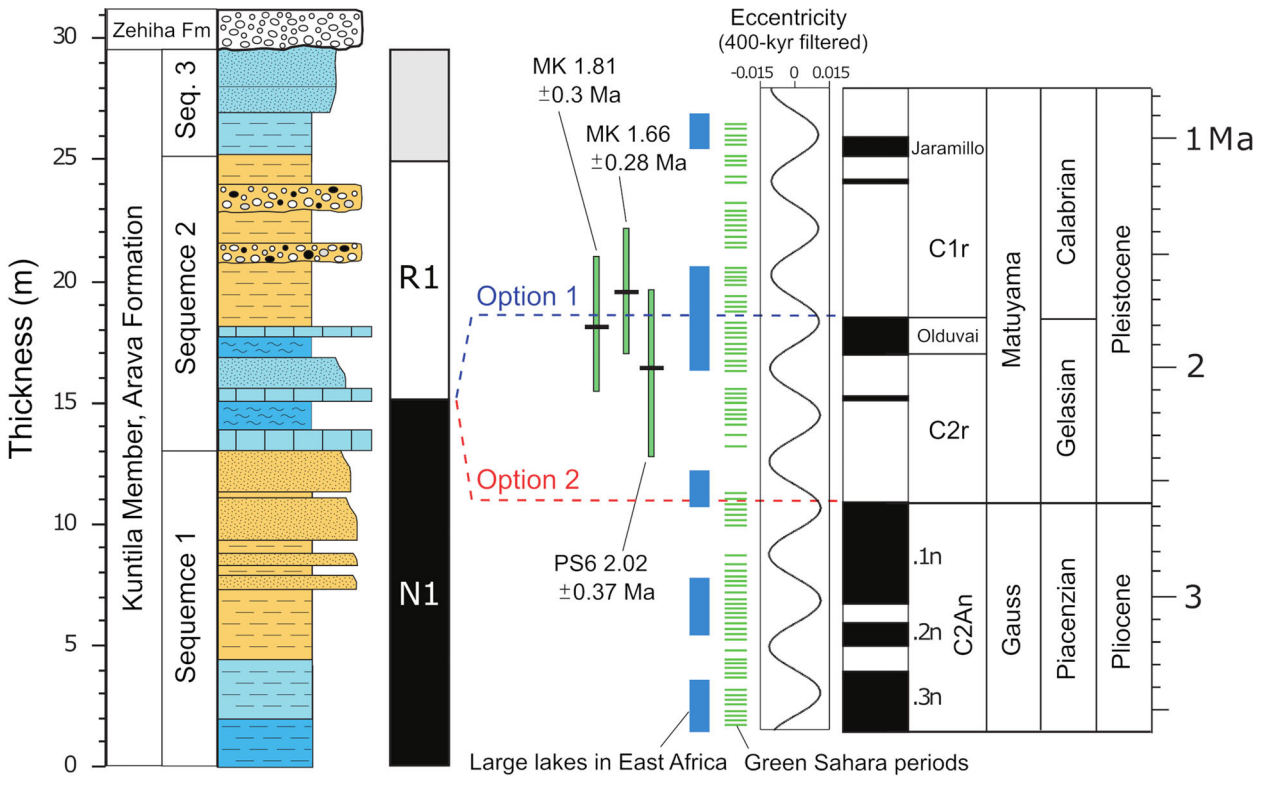

FIGURE 7 | Possible correlations of the Kuntila Lake sediments magnetostratigraphy with the astronomically-tuned Neogene times scale (ATNTS2012, Hilgen et al., 2012) taking into account the ^{10}Be exposure ages available for the top of the Arava Formation (after Guralnik et al., 2010; Amit et al., 2011). The 400-kyr band-pass filter of eccentricity (Laskar et al., 2004) is shown along with the inferred periods of large lake expansion in East Africa (Trauth et al., 2009) and clusters of Green Sahara periods (Larrasoaña et al., 2013).

It should be also noted that the 400 kyr eccentricity maxima associated with the tops of both the Olduvai and the C2An.1n Subchron are associated with protracted periods of lake expansion in East Africa (Trauth et al., 2009) and also with clusters of short-lived periods of savannah expansion throughout much of the Sahara (Larrasoaña et al., 2013; **Figure 7**). Simultaneous wetter conditions in East Africa, the Sahara and the Negev are a prerequisite for the establishment of the biogeographic connection between Africa and Eurasia that enabled the initial out-of-Africa dispersal of our genus *Homo*, whether it occurred around 1.85 Ma, as it is typically considered (Anton et al., 2014), or well before 2.12 Ma as pointed out by new evidence (Zhu et al., 2018) appears to indicate. Further research on Late Pliocene-Early Pleistocene sequences in the Levantine Corridor and surrounding areas is necessary to determine the timing and extent of African-Eurasia biogeographic connections.

CONCLUSION

Sedimentological evidence and ostracod faunas indicate that sediments of the Kuntila Member of the Arava Formation accumulated in a long-lasting lacustrine environment that underwent periodic changes in lake levels. The two lowermost sequences (S1 and S2) identified witnessed a gradual shallowing from fully lacustrine to palustrine conditions and, finally, to distal alluvial sedimentation. The third sequence identified (S3) shows a similar trend although it is devoid of the initial lacustrine part.

Magnetostratigraphic results enable recognition of a normal polarity (N1) zone in the lower half of the KG section and of a reverse polarity zone (R1) in its upper half. Correlation of the normal polarity zone to the Olduvai Subchron (1.778–1.945 Ma, Hilgen et al., 2012) appears as the most likely option in view of ^{10}Be ages derived for the uppermost part of the Kuntila Member in nearby sections (average of 1.83 Ma; Matmon et al., 2009; Guralnik et al., 2010; Amit et al., 2011). Nevertheless, the large errors associated with these cosmogenic exposure ages (typically spanning 0.6 Myr) make correlation of N1 with Subcrhon C2An.1n (2.582–3.032 Ma; Hilgen et al., 2012) also likely. Since the tops of both subchrons Olduvai and C2An.1n are associated with two 400 kyr eccentricity maxima (Laskar et al., 2004), our data unequivocally relate sedimentation of the Kuntila Lake sediments with a long period of enhanced climatic variability, driven by maxima in the Earth's eccentricity, regardless of the preferred correlation. Such enhanced climate variability drove the regional hydrological budget of the present-day hyper-arid Negev Desert to the point of enabling the formation of a long-lasting open-water surface. The 400 kyr eccentricity maxima associated with the tops of both the Olduvai and the C2An.1n Subchron also drove periods of lake expansion in East Africa (Trauth et al., 2009) and short-lived expansions of the savannah throughout much of the Sahara (Larrasoaña et al., 2013). Simultaneous wetter conditions in East Africa, the Sahara and the Negev would have generated optimal conditions for a biogeographic connection between Africa and Eurasia, facilitating initial out-of-Africa dispersal of our genus *Homo* possible. Further research on the Kuntila Lake sediments, as well as other Late Pliocene-Early Pleistocene sequences in the region, will be necessary to determine the timing and extent of such biogeographic connection between Africa and Eurasia.

DATA AVAILABILITY STATEMENT

All datasets generated for this study are included in the article/**Supplementary Material**.

AUTHOR CONTRIBUTIONS

JL performed the magnetostratigraphy and designed the research along with NW, who also led the sedimentological description of the studied sediments. SM studied the fossils. YA and HG provided the team with knowledge on the regional geological and geomorphological context. All coauthors contributed equally to fieldwork tasks and to the writing of the manuscript.

FUNDING

This study was funded by project CGL2012-30875 of the Ministerio de Economía y Competitividad of Spain and by Internal Funds of the University of Haifa.

ACKNOWLEDGMENTS

We thank Ari Matmon for assistance with cosmogenic exposure ages, Mina Weinstein-Evron for helping with the logistics for the field trip, and Bet Beamud for assistance with paleomagnetic measurements. We thank JP and JO for constructive reviews on the original manuscript.

SUPPLEMENTARY MATERIAL

The Supplementary Material for this article can be found online at: https://www.frontiersin.org/articles/10.3389/feart.2020.00173/full#supplementary-material.

TABLE S1 | Thermal demagnetization data for the studied samples.

TABLE S2 | Details on the calculation of the ChRM for the studied samples.

PLATE S1 | 1–4 *Ilyocypris* cf. *bradyi*, 1 right valve (RV) external view (ev), 2 left valve (LV) internal view (iv), 3–4 marginal ripplets on posteroventral part of inner lamella; 5 *Neglecandona angulata* ♀ carapace (cpx) slightly deformed at posterior margin; 6 *Potamocypris* sp. juvenile RV iv; 7–9 *Cyprideis torosa*, 7 ♀ cpx smooth form (*C. torosa* f. *littoralis*), 8 ♀ cpx with small nodes (arrow shows most prominent node, *C. torosa* f. *torosa*), 9 ♂ cpx smooth form. Scale bars are 50 and 250 μm. Specimens housed at Institute of Geological Sciences of Freie Universität Berlin (Germany).

PLATE S2 | 1–2 *Vestalenula cylindrica* RVs iv, 3 *Cypridopsis vidua* juvenile RV iv; 4–5 *Paralimnocythere* sp., 4 ♀ LV ev, 5 ♂ RV ev; 6–8 gyrogonites of *Chara* sp. 1, 6 apical view, 7 basal view, 8 lateral view; 9–11 gyrogonites of *Chara* sp. 2, 9 apical view, 10 basal view, 11 lateral view. Scale bar is 250 μm. Specimens housed at Institute of Geological Sciences of Freie Universität Berlin (Germany).

REFERENCES

Amit, R., Enzel, Y., Crouvi, O., Simhai, O., Matmon, A., Porat, N., et al. (2011). The role of the Nile in initiating a massive dust influx to the Negev late in the middle Pleistocene. *Geol. Soc. Am. Bull.* 123, 873–889. doi: 10.1130/b30241.1

Anton, S. C., Potts, R., and Aiello, L. C. (2014). Evolution of early Homo: an integrated biological perspective. *Science* 345:1236828. doi: 10.1126/science.1236828

Avni, Y. (1998). *Geological Evolution of the Central and Southern Negev as an Indicator of the Evolution of the Dead Sea Transform Western Margin in the Late Neogene and Quaternary*. Ph. D. Thesis, Hebrew University. Jerusalem.

Avni, Y., Bartov, Y., Garfunkel, Z., and Ginat, H. (2000). Evolution of the Paran drainage basin and its relations to the Plio-Pleistocene history of the Arava Rift western margin, Israel. *Isr. J. Earth Sci.* 49, 215–238. doi: 10.1560/w8wl-ju3y-km7w-8lx4

Avni, Y., Bartov, Y., Garfunkel, Z., and Ginat, H. (2001). The Arava formation – A pliocene sequence in the Arava Valley and its western margin, southern Israel. *Isr. J. Earth Sci.* 50, 101–120. doi: 10.1092/5u6a-rm5e-m8e3-qxm7

Avni, Y., Segev, A., and Ginat, H. (2012). Oligocene regional denudation of the northern Afar dome: pre and syn breakup stages of the Afro-Arabian plate. *Geol. Soc. Am. Bull.* 124, 1871–1897. doi: 10.1130/b30634.1

Bailey, G. N., Reynolds, S. C., and King, G. C. P. (2011). Landscapes of human evolution: models and methods of tectonic geomorphology and the reconstruction of hominin landscapes. *J. Hum. Evol.* 60, 257–280. doi: 10.1016/j.jhevol.2010.01.004

Belmaker, M. (2010). The presence of a large cercopithecine (cf. *Theropihecus* sp.) in the 'Ubeidiya formation (Early Pleistocene, Israel). *J. Hum. Evol.* 58, 79–89. doi: 10.1016/j.jhevol.2009.08.004

Deng, C., Zhu, R., Zhang, R., Ao, H., and Pan, Y. (2008). Timing of the Nihewan formation and faunas. *Quat. Res.* 69, 77–90. doi: 10.1016/j.yqres.2007.10.006

Enzel, Y., Amit, R., Dayan, U., Crouvi, O., Kahana, R., Ziv, B., et al. (2008). The climatic and physiographic controls of eatern Mediterranean over the late Pleistocene climates in the southern Levant and its neighboring deserts. *Glob. Planet. Change* 60, 165–192. doi: 10.1016/j.gloplacha.2007.02.003

Fuhrmann, R. (2012). Atlas quartärer und rezenter Ostrakoden Mitteldeutschlands. *Altenburger Naturwissenschaftliche Forschungen* 15, 1–320.

Garfunkel, Z. (1981). Internal structure of the Dead Sea leaky transform (rift) in relation to plate kinematics. *Tectonophysics* 80, 81–108. doi: 10.1016/0040-1951(81)90143-8

Ginat, H., Opitz, S., Ababneh, L., Faershtein, G., Lazar, M., Porat, N., et al. (2018). Pliocene-Pleistocene waterbodies and associated deposits in southern Israel and southern Jordan. *J. Arid Environ.* 148, 14–33. doi: 10.1016/j.jaridenv.2017.09.007

Ginat, H., Zilberman, E., and Saragusti, I. (2003). Early pleistocene lake deposits and Lower Paleolithic finds in Nahal (wadi) Zihor, Southern Negev desert, Israel. *Quaternary Res.* 59, 445–458. doi: 10.1016/s0033-5894(03)00029-2

Gradstein, F. M., Ogg, J. G., Schmitz, M. D., and Ogg, G. M. (2012). *The Geologic Time Scale*. Boston: Elsevier.

Guralnik, B. (2009). *Landscape and Tectonic Evolution of the Central Negev in Response to Dead Sea Rifting*. Ph. D. Thesis, The Hebrew University, Jerusalem.

Guralnik, B., Matmon, A., Avni, Y., and Fink, D. (2010). ^{10}Be exposure ages of ancient desert pavements reveal Quaternary evolution of the Dead Sea drainage basin and rift margin tilt. *Earth Planet. Sci. Lett.* 290, 132–141. doi: 10.1016/j.epsl.2009.12.012

Hilgen, F. J., Lourens, J. A., Van Dam, L. J., Beu, A. G., Boyles, A. F., Cooper, R. A., et al. (2012). "The Neogene period," in *The Geologic Time Scale*, eds F. M. Gradstein, J. G. Ogg, M. D. Schmitz, and G. M. Ogg (Boston: Elsevier), 923–978.

Kirschvink, J. L. (1980). The least-squares line and plane and the analysis of paleomagnetic data. *Geophys. J. R. Astron. Soc.* 62, 699–718. doi: 10.1111/j.1365-246x.1980.tb02601.x

Larrasoaña, J. C., Murelaga, X., and Garcés, M. (2006). Magnetobiocheonology of Lower Miocene (Ramblian) continental sediments from the Tudela Formation (western Ebro basin, Spain). *Earth Planet. Sci. Lett.* 243, 409–423. doi: 10.1016/j.epsl.2006.01.034

Larrasoaña, J. C., Roberts, A. P., and Rohling, E. J. (2013). Dynamics of Green Sahara periods and their role in hominin evolution. *PLoS One* 8:e76514. doi: 10.1371/journal.pone.0076514

Laskar, J., Robutel, P., Joutel, F., Gastineau, M., Correia, A. C. M., and Levrard, B. (2004). A long-term numerical solution for the insolation quantities of the Earth. *Astron. Astrophys.* 428, 261–285. doi: 10.1051/0004-6361:20041335

Lepre, C. J., Roche, H., Kent, D. K., Harmand, S., Quinn, R. L., Brugal, J. P., et al. (2011). An earlier origin for the Acheulian. *Nature* 477, 82–85. doi: 10.1038/nature10372

Matmon, A., Simhai, O., Amit, R., Haviv, I., Porat, N., McDonald, E., et al. (2009). Desert pavement-coated surfaces in extreme deserts present the longest-lived landforms on Earth. *Geol. Soc. Am. Bull.* 121, 688–697. doi: 10.1130/b26422.1

Meisch, C. (2000). *Freshwater Ostracoda of Western and Central Europe*. Heidelberg: Spektrum.

Meisch, C., Scharf, B., Fuhrmann, R., and Thiéry, A. (2019). *Neglecandona altoides* (Petkovski, 1961) nov. comb. and the genus *Neglecandona* Krstiæ, 2006 (Crustacea, Ostracoda, Candonidae). *Bull. Soc. Nat. Luxembourgeois* 121, 237–264.

Ogg, J. G. (2012). "Geomagnetic polarity timescale," in *The Geologic Time Scale*, eds F. M. Gradstein, J. G. Ogg, M. D. Schmitz, and G. M. Ogg (Boston: Elsevier), 85–113.

Orland, I. J., He, F., Bar-Matthews, M., Chen, G., Ayalon, A., and Kutzbach, J. E. (2019). Resolving seasonal rainfall changes in the middle East during the last interglacial period. *Proc. Natl. Acad. Sci. U.S.A.* 116:201903139. doi: 10.1073/pnas.1903139116

Parés, J. M., Duval, M., and Arnold, L. J. (2013). New views on an old move: hominin migration into Eurasia. *Quat. Int.* 295, 5–12. doi: 10.1016/j.quaint.2011.12.015

Pérez-Rivarés, F. J., Arenas, C., Pardo, G., and Garcés, M. (2018). Temporal aspects of genetic stratigraphic units in continental sedimentary basins: examples from the Ebro basin, Spain. *Earth Sci. Rev.* 178, 136–153. doi: 10.1016/j.earscirev.2018.01.019

Ramón, M. J., Pueyo, E. L., Oliva-Urcia, B., and Larrasoaña, J. C. (2017). Virtual directions in paleomagnetism: a global and rapid approach to evaluate the NRM components. *Front. Earth Sci.* 5:8. doi: 10.3389/feart.2017.00008

Sahnouni, M., Parés, J. M., Duval, M., Cáceres, I., Hariachane, Z., van der Made, J., et al. (2018). 1.9-million- and 2.4-million-year-old artifacts and sronetool-cutmarked bones from Ain Bucherit, Algeria. *Science* 362, 1297–1301. doi: 10.1126/science.aau0008

Toucanne, S., Minto'o, C. M. A., Fontanier, C., Bassetti, M. A., Jorry, S. J., and Jouet, G. (2015). Tracking rainfall in the northern Mediterranean borderlands during sapropel deposition. *Quat. Sci. Rev.* 129, 178–195. doi: 10.1016/j.quascirev.2015.10.016

Trauth, M. H., Larrasoaña, J. C., and Mudelsee, M. (2009). Trends, rhythms and events in Plio-Pleistocene African climate. *Quat. Sci. Rev.* 28, 399–411. doi: 10.1016/j.quascirev.2008.11.003

Vaks, A., Bar-Matthews, M., Ayalon, A., Matthews, A., Halicz, L., and Frumkin, A. (2007). Desert speleothems reveal climatic window for African exodus of early modern humans. *Geology* 35, 831–834.

van Harten, D. (1979). "Some new shell characters to diagnose the species of the *Ilyocypris gibba-biplicata-bradyi* group and their ecological significance," in *Taxonomy, Biostratigraphy and Distribution of Ostracodes*, *Proceedings of the 7th International Symposium on Ostracodes*, ed. Serbian Geological Society (Belgrade: Serbian Geological Society), 71–76.

Waldmann, N., Torfstein, A., and Stein, M. (2010). Northward intrusions of low- and mid-latitude storms across the Saharo-Arabian belt during past interglacials. *Geology* 38, 567–570. doi: 10.1130/g30654.1

Zhu, Z., Dennell, R., Huang, W., Wu, Y., Qiu, S., Yang, S., et al. (2018). Hominin occupation of the Chinese Loess Plateau since about 2.1 million years ago. *Nature* 559, 608–612. doi: 10.1038/s41586-018-0299-4

Ziv, B., Dayan, U., Kushnir, Y., Roth, C., and Enzel, Y. (2006). Regional and global atmospheric patterns governing rainfall in the southern Levant. *Int. J. Climatol.* 26, 55–73. doi: 10.1002/joc.1238

Conflict of Interest: The authors declare that the research was conducted in the absence of any commercial or financial relationships that could be construed as a potential conflict of interest.

Copyright © 2020 Larrasoaña, Waldmann, Mischke, Avni and Ginat. This is an open-access article distributed under the terms of the Creative Commons Attribution License (CC BY). The use, distribution or reproduction in other forums is permitted, provided the original author(s) and the copyright owner(s) are credited and that the original publication in this journal is cited, in accordance with accepted academic practice. No use, distribution or reproduction is permitted which does not comply with these terms.